15A.3 A POLARIMETRIC AND MICROPHYSICAL INVESTIGATION OF THE NORTHEAST BLIZZARD OF 8-9 FEBRUARY 2013

Erica M. Griffin[*,1,2,3], Alexander V. Ryzhkov[1,2], Terry J. Schuur[1,2], Heather D. Reeves[1,2], Joseph C. Picca[4], Matthew R. Kumjian[1,2,5], and Kimberly L. Elmore[1,2]

[1]Cooperative Institute for Mesoscale Meteorological Studies, University of Oklahoma
Norman, Oklahoma

[2]NOAA/OAR/National Severe Storms Laboratory
Norman, Oklahoma

[3]School of Meteorology, University of Oklahoma
Norman, Oklahoma

[4]NOAA/NWS/New York, NY National Weather Service Forecast Office
Upton, New York

[5]Advanced Studies Program, National Center for Atmospheric Research
Boulder, Colorado

1. INTRODUCTION

On 8 February 2013, two low-pressure systems merged over the northeastern United States, producing a historic winter weather event that ranked among the top five worst blizzards in the region. Figure 1 illustrates the evolution of synoptic-scale weather patterns during the event, using the 13-km Rapid Refresh (RAP; Cifelli et al. 2005) model analyses. At 1200 UTC 8 February, a closed low was located just off the North Carolina coast, and the 0°C isotherm at 2 m above ground level was located just south of Long Island, New York (Fig. 1a). At this time, precipitation associated with the low was primarily over the Mid-Atlantic States. Over the next 12 hours, the low deepened and progressed northeastward, while the precipitation shield moved over the north-Atlantic states and New England (Figs. 1b, c). By 0000 UTC 9 February, reflectivity values over Long Island were in excess of 50 dBZ. Between 0600 and 1200 UTC 9 February, the surface low moved slowly eastward and precipitation continued to fall over the New England states (Figs. 1d, e). By 1800 UTC, precipitation was no longer falling over Long Island and Connecticut (Fig. 1f).

The 24-hour accumulated liquid-equivalent precipitation, beginning at 1200 UTC 8 February, was in excess of 50 mm over Long Island and southeastern New Jersey (Fig. 2a). Accumulations exceeded 38 mm over south-central Connecticut and most of Long Island. Precipitation type observations, collected by the NOAA National Severe Storms Laboratory's Meteorological Phenomena Identification Near the Ground (mPING) project (Elmore et al. 2013), exhibited a transition of surface precipitation type between 1200 and 1800 UTC 8 February (Fig. 2b). Rain was falling over southern New Jersey, southwestern Pennsylvania, and along the southern coast of Long Island, while a narrow zone of freezing rain and ice pellets/ice pellet mixture was positioned over central New Jersey and along the northern region of Long Island. Snow was the predominant precipitation type over Connecticut, Rhode

Corresponding author address: Erica M. Griffin, CIMMS/NSSL/University of Oklahoma, School of Meteorology; National Weather Center, 120 David L. Boren Blvd., Norman, OK, 73072; email: Erica.Griffin@noaa.gov

Island, Massachusetts, and New York. As time progressed, the region of freezing rain and ice pellets shifted slightly southward (Figs. 2c, d) and eventually, most locations reported snow (Fig. 2e).

Total snow accumulations, valid at 1200 UTC 9 February, exceeded 50 cm over central Long Island, Connecticut, and Massachusetts (Fig. 2f). Heavy snowfall and blizzard conditions occurred from northern New Jersey, inland to New York, and northward through Maine (Fig. 3). Storm-total (8-9 February 2013) snow accumulations of 30-61 cm were common, with amounts surpassing 61 cm over a SW/NE-oriented band from Long Island to southern Maine. Maximum accumulations up to 102 cm, as well as snowfall rates exceeding 15 cm hr^{-1}, were reported in parts of Connecticut. In addition to record-setting snow accumulations, significant coastal flooding and hurricane-force wind gusts were recorded along the coast, with a peak gust of 40 m s^{-1}. Impacts of the event included at least 18 fatalities, thousands of flight cancellations at major airports, travel bans, and hundreds of thousands of customers throughout the region left without electricity for several days.

This study investigates the evolution and nature of intriguing and unprecedented polarimetric signatures observed during the 8-9 February blizzard, and the thermodynamic conditions within which they developed, to further understanding of the fundamental microphysical processes within winter storms. We examine data from the polarimetric WSR-88D S-band radar in Upton, NY (Long Island; KOKX) and environmental thermodynamic data from the operational 13-km RAP model. These data are used to interpret the polarimetric signatures of different types of ice crystal habits (e.g., needles, plates, stellars, and dendrites), which form in regimes of differing temperature and ice supersaturation. Additionally, polarimetric signatures are analyzed alongside surface precipitation type observations from mPING, augmented Automated Surface Observing Systems (ASOS) stations, and observations from the Stony Brook, New York (SBNY) NWS forecast office; these data allowed for verification of radar-indicated winter precipitation types.

2. BACKGROUND

Currently, the microphysical properties of winter storms have largely been unexplored, as polarimetric investigations have focused primarily on warm-season and severe convective storms. Yet, with the recent polarimetric upgrades to the United States WSR-88D network, ample dual-polarization data is now available for locations throughout the country, allowing for abundant observations of the microphysical properties of winter precipitation. Recently, unique and fascinating polarimetric signatures in winter storms have been discovered. Andrić et al. (2009, 2010, 2013) have documented enhanced differential reflectivity (Z_{DR}) signatures located above the environmental freezing layer, along with enhancements in specific differential phase (K_{DP}) and slightly reduced co-polar correlation coefficient (ρ_{hv}). These elevated signatures appeared in horizontal layers or isolated “pockets” and were also associated with Z_H increasing toward the ground (Andrić et al. 2013). The enhanced Z_{DR} values signified the presence of large, horizontally-oriented ice crystals in the subfreezing temperatures aloft (between -10 and -15°C), believed to be primarily due to dendritic growth (Andrić et al. 2010). Furthermore, Kennedy and Rutledge (2011) documented the occurrence of elevated layers of enhanced K_{DP} (~0.15-0.4°km^{-1}) near the -15°C temperature level, during intense precipitation periods of winter storms. These signatures were collocated with regions of significant depositional growth of dendritic ice particles.

Ryzhkov et al. (2011) presented a preliminary examination of distinct and recurring polarimetric signatures in winter storms, including the aforementioned elevated features, providing inspiring groundwork for future winter weather polarimetric studies. As recognized by Hogan et al. (2002) and Field et al. (2004), “plumes” of enhanced Z_{DR} are associated with updrafts and generation of supercooled liquid water in winter convective storms. According to Ryzhkov et al. (2011), it is likely that some of these updrafts can produce enough graupel for charge separation sufficient to generate electric fields. Furthermore, these electrostatic fields can change the orientation of ice crystals atop these updrafts, which can cause the transmitted radar signal to become depolarized (Ryzhkov and Zrnić 2007; Ryzhkov et al. 2011). The resulting polarimetric signatures reveal the depolarization through radial streaks of enhanced positive and negative Z_{DR}.

Other distinct polarimetric signatures presented by Ryzhkov et al. (2011) include melting layer bright-band “downward excursions,” characterized by reduced ρ_{hv} and locally-maximized Z_H and Z_{DR} extending from the melting layer down to the surface. These signatures have been associated with abrupt changes in precipitation type reaching the ground (Ryzhkov et al. 2011), which present a challenge to forecasters. Therefore, polarimetric radar observations of this phenomenon would prove useful in winter weather nowcasting.

The most recently documented polarimetric feature is the “refreezing signature,” which forms in the lower levels below the melting layer bright-band and is characterized by enhanced Z_{DR} and K_{DP}, and reduced Z_H and ρ_{hv}. Kumjian et al. (2013) observed this signature and associated environmental conditions in four winter storms over central Oklahoma, using the S-band polarimetric WSR-88D KOUN radar in Norman, Oklahoma and the University of Oklahoma’s C-band Polarimetric Radar for Innovations in Meteorology and Engineering (OUPRIME). During the events, the refreezing signature occurred when ice pellets were reaching the surface (Kumjian et al. 2013). The low-level Z_{DR} enhancement is likely indicative of substantial refreezing of precipitation particles, as well as the production of anisotropic ice crystals (Kumjian et al. 2013). Further analysis is needed to thoroughly understand the origin of the ice crystals, as well as to explain the microphysical processes responsible for the occurrence of this unique polarimetric feature. Nevertheless, the refreezing signature will be valuable in detecting transitions of precipitation from freezing rain to ice pellets/sleet (Ryzhkov et al. 2011; Kumjian et al. 2013).

3. OBSERVATIONAL ANALYSIS

Here, we present a selection of intriguing dual-polarization radar observations of the Northeast blizzard, during the observational period of 1000 UTC 8 February 2013 through 0400 UTC 9 February 2013, which included the onset, intensification, and initial dissipation phases of the system.

3.1. High, Shallow Z_H near Surface

Z_H during this event was unprecedented for a winter storm, reaching as high as 60 dBZ in regions of wet snow near the surface. This system was extraordinary, considering Z_H values in winter storms are typically no greater than ~40 dBZ (Ganetis et al. 2013). The exceptionally-large Z_H (> 50 dBZ) was confined to a shallow layer below 1.5 km throughout the entire observational period (e.g., Fig. 4). Also, Z_H contours greater than 24 dBZ remained below approximately 6 km (e.g., Fig. 4).

As the convection intensified, Z_H near the surface increased, especially after 2100 UTC 8 February. The incoming precipitation bands (comma-head precipitation) became more north/south oriented after 2200 UTC, while retaining large Z_H (60 dBZ; Fig. 5a). Figure 5a-c (2216 UTC 8 February) displays the state of precipitation during this period, with pure dry snow (Z_H < 35 dBZ, 0-0.5 dB, and ρ_{hv} near 1) within colder temperatures north of the model- indicated 0°C isotherm, and wet snow/mixed-phase hydrometeors (freezing rain/ice pellets/snow; 40-60 dBZ, 1.25-3.5 dB, and ρ_{hv} as low as 0.75) within warmer temperatures south of the 0°C line. There was a nearly horizontal transition from the enhanced Z_{DR} and ρ_{hv} values to the small Z_{DR} and high ρ_{hv} values (Fig. 5b,c), distinctly indicating the location of the "true" 0°C isotherm. While the location of the 0°C transition line was exceptionally distinct in polarimetric imagery, the overlaid RAP model-indicated wet-bulb temperatures did a less accurate job detecting local temperature perturbations (Fig. 5b,c).

As time progressed, the region of maximum Z_H (> 50 dBZ) shifted north of KOKX (over Connecticut), and north of the 0°C isotherm (e.g., Fig.5d; 0236 UTC 9 February), into colder temperatures. After the main snowband traversed north of the 0°C isotherm, dry snow became the predominant precipitation type, while ice pellets were also observed at the surface, south of the transition line (Fig. 5d-f). Curiously, despite the intense convection residing within negative surface temperatures, wet snow was observed in the maximum Z_H region (Fig. 5d-f). This could possibly be attributed to local warming due to anomalously-heavy snow falling through the melting layer, and then reaching the surface before refreezing entirely. The polarimetric variables illustrate a more north/south-oriented transition line than at 2216 UTC, while the RAP model did not detect the smaller-scale temperature perturbations. Considering the polarimetric data captured the local temperature deviations more accurately than the RAP model, dual-polarization radar data could be a valuable tool for forecasters, when nowcasting transitional winter weather precipitation.

3.2. Differential Attenuation

One of the most prominent features of the event was the remarkable differential attenuation, which resulted from the radar beam propagating through regions of heavy, wet snow. This polarimetric signature occurred throughout the entire observational period, becoming more distinct as the convection intensified. The 1.45° PPI Z_{DR} imagery at 0001 UTC 9 February (Fig. 6) displays the differential attenuation, indicated by Z_{DR} values of -2 to 0 dB, southwest and northeast of KOKX. These negative Z_{DR} values occurred down-radial of regions of mixed-phase hydrometeors, including heavy wet snow, ice pellets, as well as some "anomalous" ice hydrometeors which had the appearance of sleet/crystals captured within a larger volume of clear, non-spherical ice (exhibiting wet growth/hail-like formation); the mixed-phase precipitation regions at this elevation were indicated by Z_H up to 57 dBZ, Z_{DR} up to 3 dB, and ρ_{hv} as low as 0.75 (Fig. 6) within a 50 km range of the radar. Figure 7 displays an example image of the anomalous large ice hydrometeors (or "asteroid" ice), appearing heavily rimed when observed at SBNY at 0043 UTC (Ganetis et al. 2013). Diversity in ice crystals during this phase of the system was illustrated in the image of columns, needles, and sleet at 0147 UTC (Fig. 8).

The 216° RHI plots in Fig. 9, at 2233 UTC 8 February, further illustrate the differential attenuation down-radial of the heavy wet snow and mixed precipitation which were located in regions of Z_H up to 57 dBZ, Z_{DR} up to 3.5 dB, and ρ_{hv} as low as 0.75 (located below 1.5 km; Fig. 9). The reduced Z_{DR} values occurred within a layer above the shallow precipitation, at approximately 1-3 km (Fig. 9). Also, the differential propagation phase (Φ_{DP}) rapidly accumulated down-radial of the heavy wet snow region, exceeding 100° (Fig. 9). Figure 10 displays a line plot of the values of Φ_{DP}, Z_{DR}, and ρ_{hv} as functions of range, at the 2.4° elevation scan along the 2233 UTC 216° azimuth. Beginning at a range of ~10 km, there was a rapid increase in Φ_{DP}, with values reaching 125° at 100 km (Fig. 10), providing further evidence of the large snowflakes/hydrometeors in the heavy precipitation. Z_{DR} peaked at ~2.7 dB (due to the beam passing through the wet snow region with the largest Z_H values) and then decreased and remained mostly negative over a large range beyond approximately 30 km (Fig. 10). ρ_{hv} was reduced at ranges between 10 and 35 km, when the beam propagated through the wet snow and mixed-phase precipitation at the lower heights near the surface (Fig. 10).

3.3. Melting Layer Bright Band Downward Excursion

As the second snowband approached Long Island from the south, a semi-circular shape in the polarimetric ρ_{hv} and Z_{DR} signatures became evident by 1300 UTC 8 February (e.g., 1354 UTC; Fig. 11), indicating a downward excursion of the melting layer bright band (MLBB) to the surface. Figure 12 provides a range versus height schematic of the melting layer sloping downward toward the surface.

As time progressed, a “bubble-like” feature became evident in Z_{DR} and ρ_{hv} imagery, located slightly northeast of KOKX; it was attached to the MLBB semi-circle and curiously fluctuated in size and distance from the semi-circle during approximately three hours. The “bubble” was characterized by enhanced Z_{DR} (1-2.5 dB) and reduced ρ_{hv} (as low as 0.9), and was first observed just after 1400 UTC, while the semi-circle MLBB-to-ground signature was becoming progressively more distinct with elevation and time. By 1459 UTC, the bubble had become larger and more distinct (Fig. 13). Eventually, it began to detach from the semi-circle, becoming nearly completely detached by 1557 UTC (Fig. 14). By 1659 UTC, the bubble had nearly completely dissipated, leaving the semi-circular-shaped MLBB-to-ground signature with a more distinct horizontal line of reduced ρ_{hv} and enhanced Z_{DR} (Fig. 15). By 1900 UTC, the downward excursion of the MLBB had become less distinct, as heavy precipitation bands moved northward and meshed with the semi-circle, appearing as a widespread region of precipitation with a horizontal leading line.

The polarimetric detection of the MLBB extension to the surface was verified by an observed transition of surface precipitation types (Fig. 2b). Rain was falling over the southern coast of Long Island, while a narrow zone of freezing rain and ice pellets/ice pellet mixture was positioned along the northern region of Long Island. After the dissipation of the polarimetric signature, the region of freezing rain and ice pellets shifted slightly southward (Figs. 2c,d).

3.4. Dendritic Growth

Elevated horizontal layers or “patches” of enhanced Z_{DR}, $K_{DP,}$ and reduced ρ_{hv} were observed above the environmental freezing layer, within the comma-head region of the cyclone. The enhanced Z_{DR} likely signified rapid depositional growth of large, horizontally-oriented dendritic ice crystals at the subfreezing temperatures aloft. Further aggregation of large dendrites causes a decrease of Z_{DR} below. Figure 16 illustrates this intriguing feature along the 0° azimuth at 0305 UTC 9 February. Enhanced Z_{DR} (1-3 dB), K_{DP} (up to 2 °km^{-1}), and ρ_{hv} (as low as 0.9) were observed in a layer above ~3 km, within the model-indicated -12 and -25°C wet-bulb temperature isotherms (Fig. 16). The largest K_{DP} values were preferentially located between the -14 and -18°C isotherms and there was a pronounced vertical Z_H

gradient directly below the layer. Also at this time, Z_H near the surface exceeded 50 dBZ, while exceptionally-heavy snow (fine, low-density snow with little rime) was observed at the surface.

These dendritic growth layers were first observed after 1200 UTC 8 February, as much as 10 hours prior to the greatest Z_H values near the surface and the most intense convective period. As time progressed, and as Z_H exceeded 50 dBZ as convection intensified, the layers became more evident and occurred above the regions of large Z_H. By 2100 UTC, the layers had become yet more evident (particularly K_{DP}) as Z_H further increased in the heavy snowband and as colder and drier air was introduced. The layers were less visible between 2300 UTC 8 February and 0100 UTC 9 February, but reappeared and became most distinct from 0100-0400 UTC, particularly north of KOKX, above the greatest Z_H values over Connecticut.

Overall, it appears the dendritic growth layers were correlated with the increase in heavy snowfall; dendritic ice crystals were generated aloft, became aggregated, fell downward toward the earth, and then contributed to the large Z_H values near the surface. The layers appeared increasingly more evident as the period of most intense convection neared, with the initial layer observations preceding the greatest surface Z_H values by several hours. Additionally, throughout the event, K_{DP} values of 0.5-2°km^{-1} (and as large as 5°km^{-1}) were persistently observed in the vicinity of the -15°C wet-bulb temperature level and were most enhanced during the intense convective periods, bolstering the results of Kennedy and Rutledge (2011) and Andrić et al. (2009, 2010, 2013).

The dendritic growth layers were particularly apparent in PPI plots above the 6° elevation scans. Figure 17 (2106 UTC 8 February) displays a striking example of double rings of enhanced Z_{DR}, reduced ρ_{hv}, and slightly enhanced K_{DP} encircling KOKX; the outer ring indicates the dendritic growth layer (between approximately -10 and -20°C), while the inner ring indicates the MLBB. The dendritic growth layer occurred at greater heights southeast of KOKX, where temperatures were warmer at the surface, while the layer occurred at lower heights northwest of KOKX, above colder surface temperatures. At this time, surface precipitation type reports consisted of snow, wet snow, and ice pellets. Also at this time, and during the following hour, large dendrites/aggregates within the heavy snow were observed along the North Shore. Lightly-rimed dendrites were falling at SBNY, as demonstrated in the photograph taken at 0409 UTC (Fig. 18). Note that this signature (Fig. 17) preceded the rapid increase in Z_H near the surface (60 dBZ) by less than one hour.

3.5. Informative Polarimetric Artifacts

Several types of artificial signatures were observed in the polarimetric data. These features should not be overlooked, as they can provide valuable information about storm microphysical processes.

a. Depolarization Streaks

Depolarization streaks were observed during the most intense convective period of the event. According to Ryzhkov et al. (2011), weak convective updrafts in winter storms can produce a tangible amount of graupel and charge separation sufficient to generate electric fields. Furthermore, strong electrostatic fields can change the orientation of ice crystals atop these updrafts, causing the transmitted radar signal to become depolarized (Ryzhkov and Zrnić 2007, Ryzhkov et al. 2011). The resulting polarimetric signatures reveal the depolarization through radial streaks of enhanced positive and negative Z_{DR}. Therefore, the numerous depolarization streaks observed during the Northeast blizzard event provided evidence of strong atmospheric electrification.

Depolarization streaks occurred beneath the comma-head region of the synoptic-scale low-pressure system from 2100 UTC 8 February through 0300 UTC 9 February, and were most distinct and ubiquitous during the 2300 UTC hour, when Z_H exceeded 55 dBZ near the surface. The streaks were observed at the 0.5-9.89° elevation angles, especially at 1.45-4.3°, and originated at uncharacteristically-low heights atop weak convective updrafts in regions of heavy, wet snow. Origination heights ranged from 1-5 km, but were primarily at approximately 3 km. Average origination heights were slightly lower after 0000 UTC, when compared to those prior to 0000 UTC. The PPI image at 2314 UTC 8 February (Fig. 19) provides an example of the streaks observed during the event. The Z_{DR} imagery displays radial streaks of enhanced positive and negative Z_{DR}, exceeding 5 dB and -2 dB, respectively. The streaks originated atop weak convective updrafts in regions of heavy wet snow (Z_H as large as 60 dBZ, ρ_{hv} as low as 0.9).

b. Non-Uniform Beam Filling

A second type of artificial polarimetric signature observed was non-uniform beam filling (Ryzhkov 2007), revealed by a wedge of radial streaks of reduced ρ_{hv} (e.g., Fig. 20). This region of low ρ_{hv} indicates large vertical gradients of Φ_{DP}, due to a non-uniform mixture of precipitation types and sizes within the radar beam cross-sections. Here, the diverse precipitation types were likely heavy snow and ice crystals.

c. "Snow Flare"

Lastly, a "snow flare" was observed northeast of KOKX from 0000-0200 UTC 9 February at the 6°-19.5° elevation scans, revealed by enhanced values of ρ_{hv} and Z_{DR}, collocated with low Z_H and moderate K_{DP} (e.g., Fig. 21). The signature flared outward from the radar and appeared similar to a three-body scattering signature, which is correlated with the presence of hailstones. However, in this case, the signature appears to have been associated with very large snowflakes and ice hydrometeors (e.g., Zrnić 1987; Hubbert and Bringi 2000; Kumjian et al. 2010; Zrnić et al. 2010; Picca and Ryzhkov 2012). The flare was correlated with observations of heavy snow, wet snow, and ice pellets at the surface. Also, surface observations at SBNY included rimed snow and large, "anomalous" ice hydrometeors ("asteroid" ice; Fig. 7). As the flare began to appear less distinct, wet-growth ice hydrometeors were on a downward trend, with a decreasing density of rimed snow from SBNY toward the North Shore. During the hour following the disappearance of this signature, heavy, much less dense snow (with some aggregates) was observed at SBNY and the surrounding areas, while there was a rapid decrease in sleet/graupel/heavily rimed snow.

4. CONCLUSIONS

The Northeast blizzard of 2013 was a unique event, exhibiting several intriguing dual-polarization radar signatures. This study investigated the evolution and nature of these sometimes unprecedented signatures, and the thermodynamic conditions within which they developed, to develop a better understanding of the fundamental microphysical processes within winter storms. Polarimetric data (from the S-band KOKX radar) were analyzed alongside RAP model wet-bulb temperatures, as well as surface precipitation type observations from mPING, augmented ASOS stations, and the Stony Brook, New York NWS forecast office; these data allowed for verification of radar-indicated winter precipitation types.

Z_H values during this event were extraordinary for a winter storm, reaching as much as 60 dBZ within a shallow layer just above the surface throughout the entire observational period. Also, as the incoming snowbands proceeded northward, the 0°C transition line was exceptionally distinct in polarimetric imagery, while the RAP model did a less-accurate job detecting local temperature perturbations. Since the polarimetric data captured local temperature perturbations more accurately than the RAP model, dual-polarization radar data could be a valuable tool for forecasters, when nowcasting transitional winter weather precipitation. Another prominent feature of the event was the remarkable differential attenuation, resulting from the radar beam propagating through regions of heavy wet snow and mixed-phase precipitation. The attenuation became more distinct as the convection intensified. This study also observed a downward excursion of the MLBB to the surface, characterized by reduced ρ_{hv} and locally-maximized Z_H and Z_{DR}; this feature was correlated with a transition line of precipitation types at the surface.

Some of the most distinctive signatures observed during the event were elevated horizontal layers or “patches” of enhanced Z_{DR}, K_{DP}, and reduced ρ_{hv} located above the environmental freezing layer, within the comma-head region of the cyclone. The enhanced Z_{DR} values likely signified the presence of large, horizontally-oriented dendritic ice crystals at the subfreezing temperatures aloft, within the temperature interval -10 to -15°C, where the conditions for rapid depositional growth are most favorable. These dendritic growth layers were correlated with the increase in heavy snowfall; dendritic ice crystals were generated aloft, became aggregated, fell downward, and then contributed to the large Z_H values near the surface. The layers appeared increasingly more evident as the period of most intense convection neared, with the initial layer observations preceding the greatest surface Z_H by several hours.

Several artificial polarimetric signatures were also observed, and provided valuable information about the system’s microphysical processes. Depolarization streaks were distinct and ubiquitous during the event’s most intense convective period, when Z_H exceeded 55 dBZ near the surface. These radial streaks of positive and negative Z_{DR} indicated regions of strong atmospheric electrification and originated at uncharacteristically-low heights, atop weak convective updrafts in regions of heavy wet snow. The effects of non-uniform beam filling were also observed during the event, indicating large gradients of Φ_{DP} within the radar resolution volume, due to a non-uniform mixture of precipitation types and sizes within the radar beam cross-sections. Lastly, a “snow flare” of enhanced ρ_{hv} and Z_{DR}, moderate K_{DP}, and low Z_H flared outward from the radar and appeared similar to a three-body scattering signature. This feature was associated with very large snowflakes and ice hydrometeors at the surface, including heavy wet snow, ice pellets, rimed snow, and large, “anomalous” ice hydrometeors known as “asteroid” ice.

Currently, the microphysical properties of winter storms have largely been unexplored, as polarimetric investigations have been focused on warm-season and severe convective storms. This study provides a next step towards understanding the fundamental microphysical processes within winter precipitation. The radar signatures investigated in this study convey the value of polarimetry in identifying features undetectable in conventional radar data. These signatures are associated with hazardous winter weather conditions that cause havoc on the public and transportation, both at the surface and in the air. Therefore, polarimetry provides a valuable tool for short-term detection and prediction of winter weather precipitation types, especially transitional events.

5. ACKNOWLEDGEMENTS

Funding was provided by NOAA/Office of Oceanic and Atmospheric Research under NOAA-University of Oklahoma Cooperative Agreement #NA11OAR4320072, U.S. Department of Commerce, and by the U.S. National Weather Service, Federal Aviation Administration, and Department of Defense program for modernization of NEXRAD radars.

6. REFERENCES

Andrić, J., D. S. Zrnić, and V. M. Melnikov, 2009: Two-layer patterns of enhanced ZDR in clouds. Extended Abstracts, 34th Conf. on Radar Meteorology, Williamsburg, VA, Amer. Meteor. Soc., P2.12. [Available online at http://ams.confex.com/ams/pdfpapers/155481.pdf].

Andrić, J., D. S. Zrnić, J. M. Straka, and V. M. Melnikov, 2010: The enhanced ZDR signature in stratiform clouds above melting layer. Extended Abstracts, 13th Conf. on Cloud Physics, Amer. Meteor. Soc., Portland, Oregon, P2.89. [Available in the online archive of the AMS].

Andrić, J., M. R. Kumjian, D. S. Zrnić, J. M. Straka, and V. M. Melnikov, 2013: Polarimetric signatures above the melting layer in winter storms: An observational and modeling study. *J. Appl. Meteor. Clim.,* **52,** 682–700.

Cifelli, R., N. Doesken, P. Kennedy, L.D. Carey, S.A. Rutledge, C. Gimmestad, and T. Depue, 2005: The community collaborative rain, hail, and snow network: Informal education for scientists and citizens. *Bull. Amer. Meteor. Soc.,* **86,** 1069-1077.

Elmore, K. L., Z. L. Flamig, V. Lakshmanan, B. T. Kaney, V. Farmer, and L. P. Rothfusz, 2013: mPING: Crowd-Sourcing Weather Reports for Research. *Bull. Amer. Meteor. Soc.,* in press.

Ganetis, S. A., B. A. Colle, M. J. Sienkiewicz, D. M. Schultz, P. L. Heinselman, and D. R. Novak, 2013: Evolution of an intense mesoscale snowband during the 8–9 February 2013 Northeast U.S. blizzard. Oral Presentation, 15th Conf. on Mesoscale Processes, Portland, OR, Amer. Meteor. Soc., P16.5. [Available online at https://ams.confex.com/ams/15MESO/flvgateway.cgi/id/24853?recordingid=24853].

Field, P., R. Hogan, P. Brown, A. Illingworth, T. Choularton, P. Kaye, E. Hirst, and R. Greenway, 2004: Simultaneous radar and aircraft observations of mixed-phase cloud at the 100 m scale. *Quart. J. Roy. Meteor. Soc.,* **139**, 1877-1904.

Hogan, R., P. Field, A. Illingworth, R. Cotton, and T. Choularton, 2002: Properties of embedded convection in warm-frontal mixed-phase cloud from aircraft and polarimetric radar. *Quart. J. Roy. Meteor. Soc.,* **128**, 451-476.

Hubbert, J., and V. N. Bringi, 2000: The effects of three-body scattering on differential reflectivity signatures. *J. Atmos. Oceanic Technol.,* **17**, 51–61.

Kennedy, P. C., and S. A. Rutledge, 2011: S-band dual-polarization radar observations of winter storms. *J. Appl. Meteor. Clim.,* **50**, 844-858.

Kumjian, M., J. C. Picca, S. M. Ganson, A. V. Ryzhkov, and D. S. Zrnic´, 2010: Three-body scattering signatures in polarimetric radar data. NOAA/NSSL Rep., 12 pp. [Available online at http://publications.nssl.noaa. gov/wsr88d_reports/FINAL_TBSS.doc.]

Kumjian, M., A. Ryzhkov, H. Reeves, and T. Schuur, 2013: A dual-polarization radar signature of hydrometeor refreezing in winter storms. *J. Appl. Meteor. Climatol.* doi:10.1175/JAMC-D-12-0311.1, in press.

Picca, J., A. Ryzhkov, 2012: A Dual-Wavelength Polarimetric Analysis of the 16 May 2010 Oklahoma City Extreme Hailstorm. *Mon. Wea. Rev.*,**140**, 1385–1403.

Ryzhkov, Alexander V., 2007: The Impact of Beam Broadening on the Quality of Radar Polarimetric Data. *J. Atmos. Oceanic Technol.*, **24**, 729–744.

Ryzhkov, A. V., and D. S. Zrnić, 2007: Depolarization in ice crystals and its effect on radar polarimetric measurements. *J. Atmos. Oceanic Technol.,* **24**, 1256-1267.

Ryzhkov, A., H. Reeves, T. Schuur, M. Kumjian, and D. Zrnić, 2011: Investigations of polarimetric radar signatures in winter storms and their relation to aircraft icing and freezing rain. Extended Abstracts, 35th Conf. on Radar Meteorology, Pittsburgh, PA, Amer. Meteor. Soc., P13.197. [Available online at https://ams.confex.com/ams/35Radar/webprogram/Paper191245.html].

Zrnić, D. S., 1987: Three-body scattering produces precipitation signature of special diagnostic value. *Radio Sci.,* **22,** 76-86.

Zrnić, D. S., G. Zhang, V. Melnikov, J. Andric, 2010: Three-Body Scattering and Hail Size. *J. Appl. Meteor. Climatol.*, **49**, 687–700.

7. FIGURES

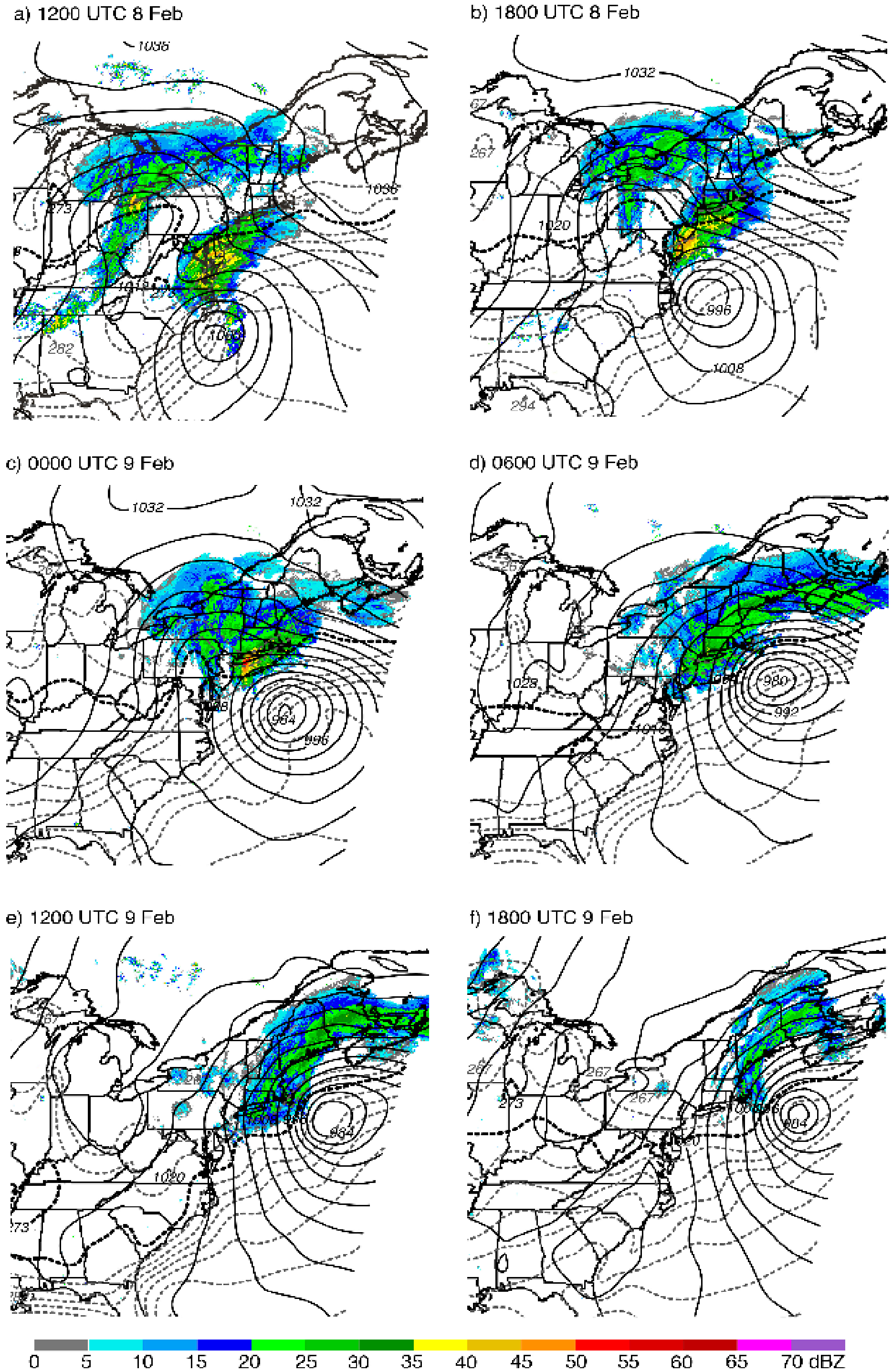

Fig.1: The observed mosaic of composite reflectivity (shaded) and Rapid-Refresh analyses of sea-level pressure (hPa; solid) and 2 m temperature (dashed). The 273 K (0°C) isotherm is bold-faced.

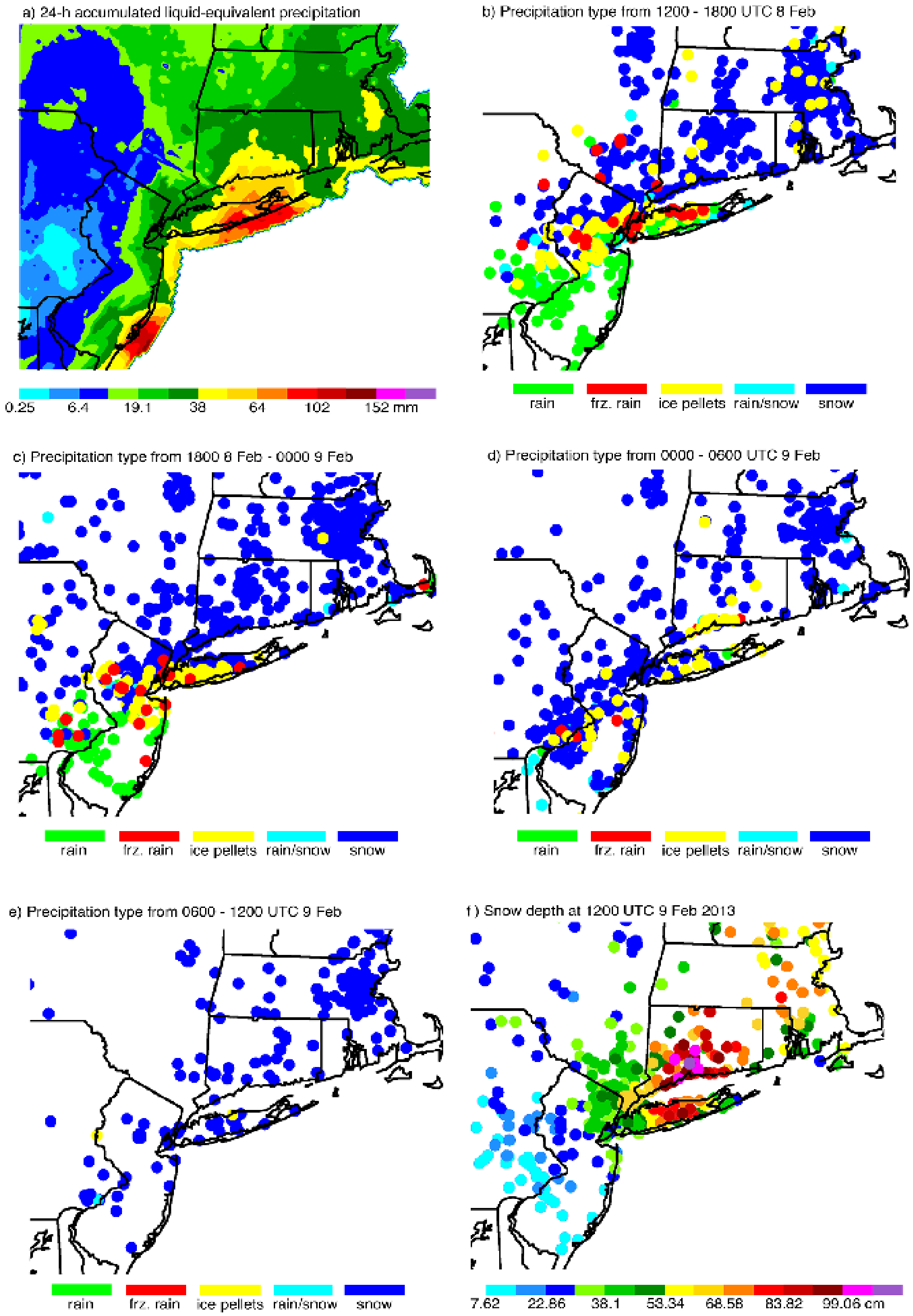

Fig. 2: The (a) stage-IV analyzed liquid-equivalent 24 hour accumulated precipitation beginning at 1200 UTC 8 February, (b-e) observed precipitation type, and (f) snow depth observations from NWS observers and CoCoRaHS (Cifelli et al. 2005).

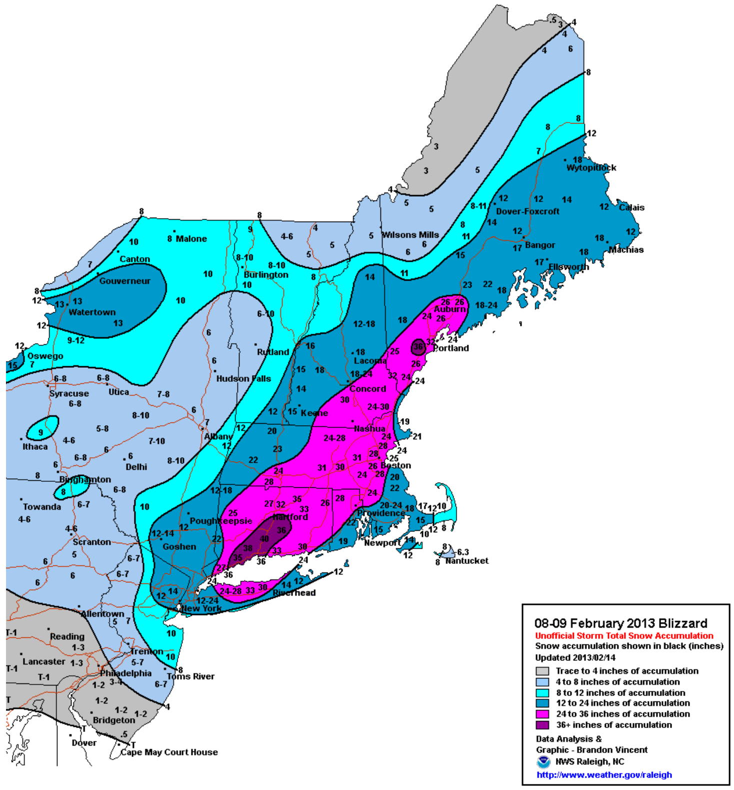

Fig. 3: 8-9 February 2013 blizzard storm-total snow accumulation (http://www.weather.gov/raleigh).

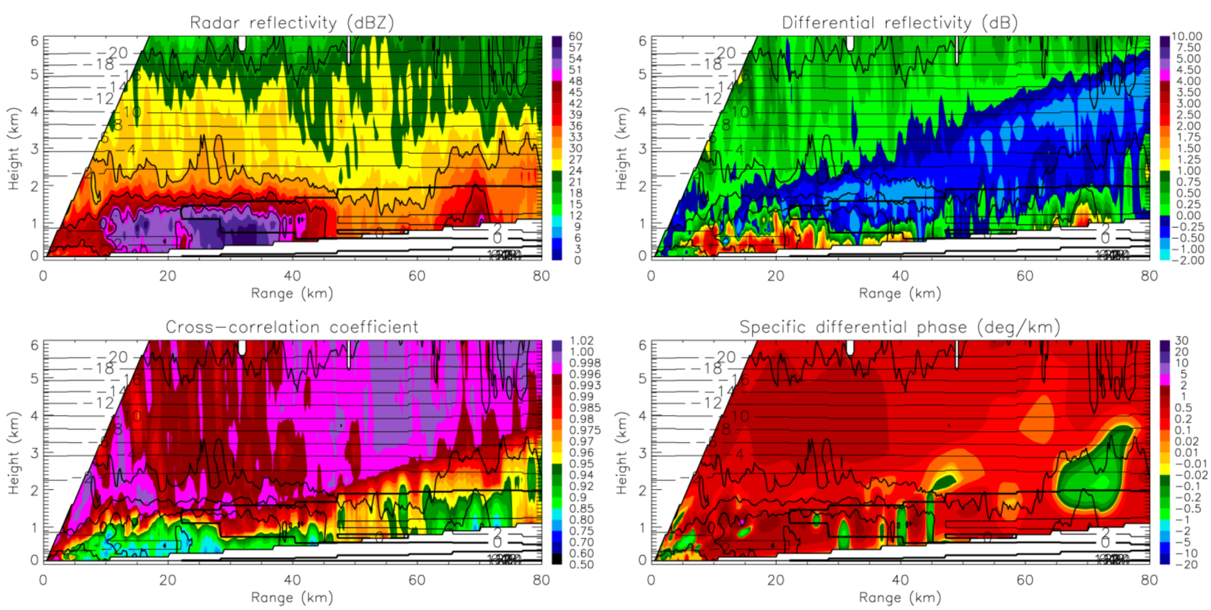

Fig. 4: RHIs of Z_H, Z_{DR}, ρ_{hv}, and K_{DP} (top left/right, bottom left/right, respectively) at 2216 UTC 8 February 2013, at 144° azimuth.

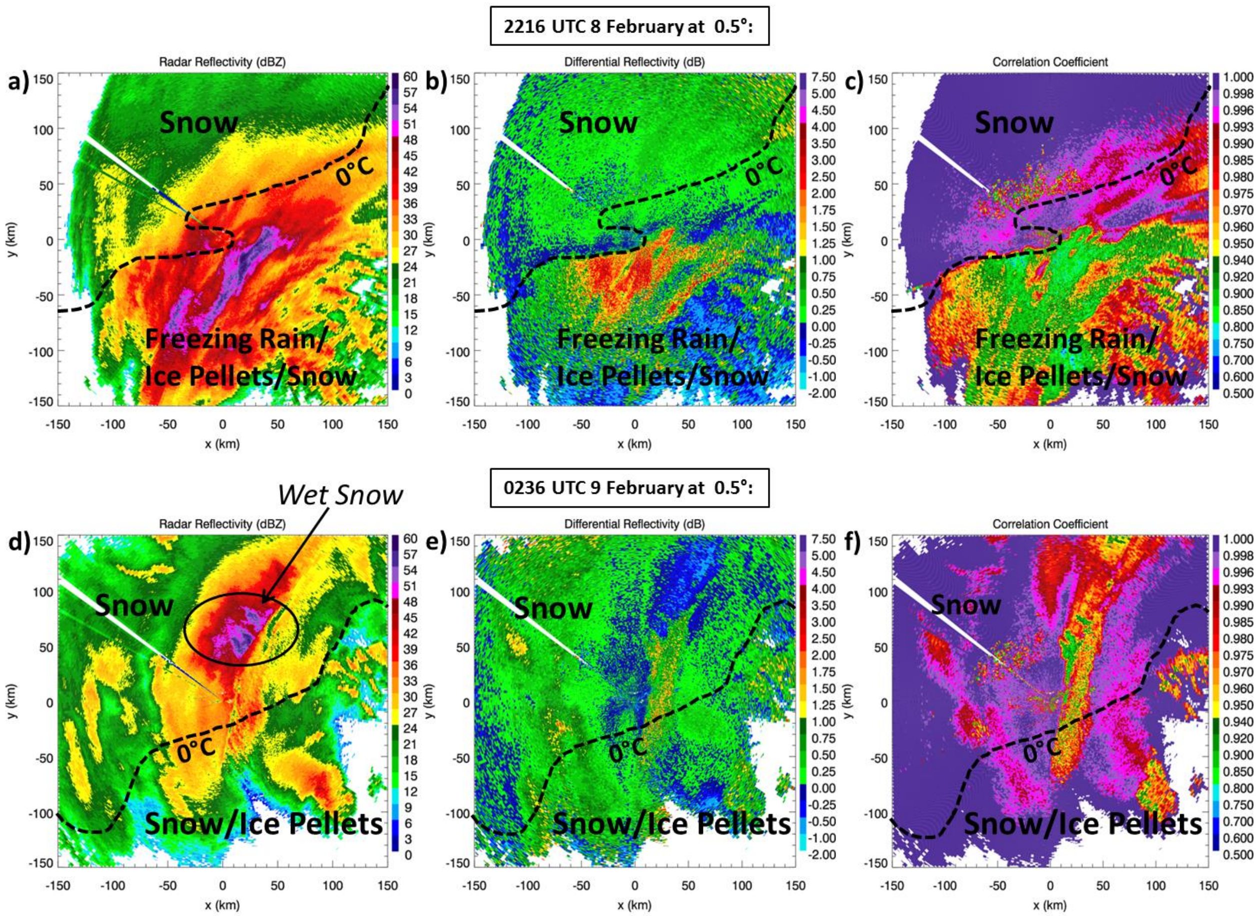

Fig.5: PPI displays of the polarimetric variables at (a-c) 2216 UTC 8 February and (d-f) 0236 UTC 9 February, at 0.5° elevation. The 0°C RAP model wet-bulb temperature at the surface is overlaid (bold, dashed contour). a-c) At 2216 UTC, pure dry snow was located within colder temperatures north of the 0°C isotherm, while wet snow/mixed-phase hydrometeors occurred within warmer temperatures south of the 0°C line. d-f) At 0236 UTC, dry snow was predominant, while ice pellets were also observed at the surface, south of the transition line. Also, wet snow was observed in the maximum Z_H region within negative surface temperatures, north of the 0°C contour.

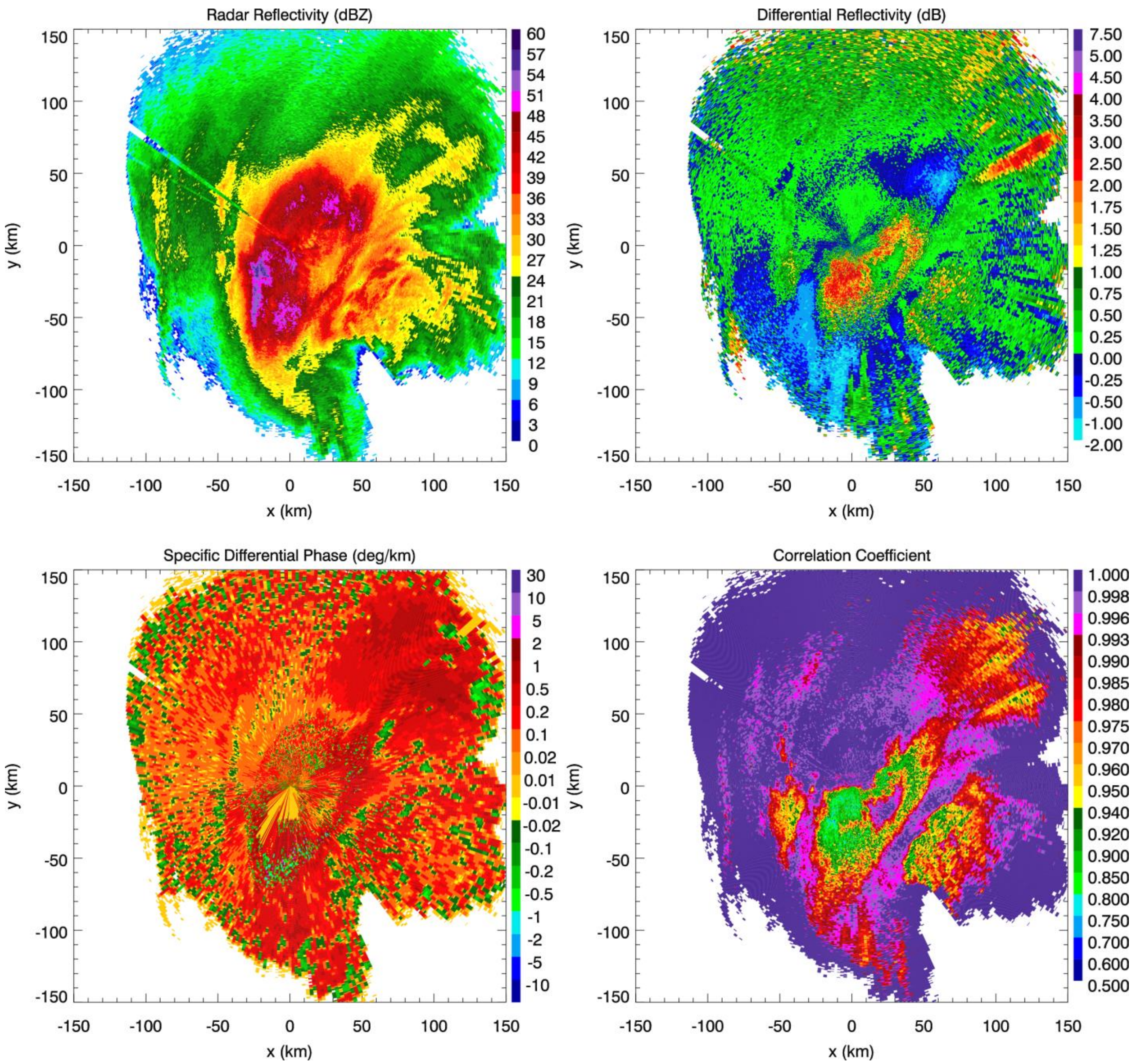

Fig.6: PPIs of Z_H, Z_{DR}, K_{DP}, and ρ_{hv} (top left/right, bottom left/right, respectively) at 0001 UTC 9 February 2013, at 1.45° elevation.

Fig.7: Image of a large, "anomalous" ice hydrometer (or "asteroid" ice), observed at the surface at 0043 UTC 9 February at SBNY (Ganetis et al. 2013).

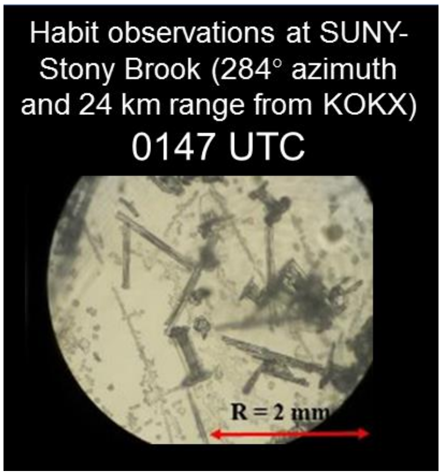

Fig.8: Image of the diverse ice-crystal types (columns, needles, and sleet), observed at the surface at 0043 UTC 9 February at SBNY (Ganetis et al. 2013).

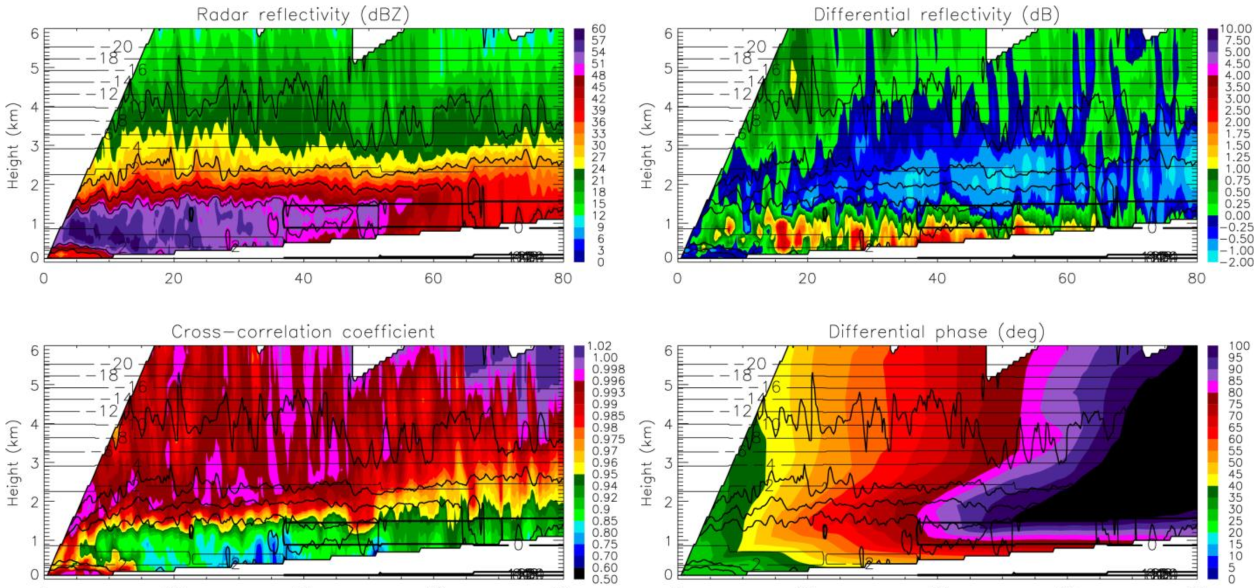

Fig.9: RHIs of Z_H, Z_{DR}, ρ_{hv}, and Φ_{DP} (top left/right, bottom left/right, respectively) at 2233 UTC 8 February 2013, at 216° azimuth.

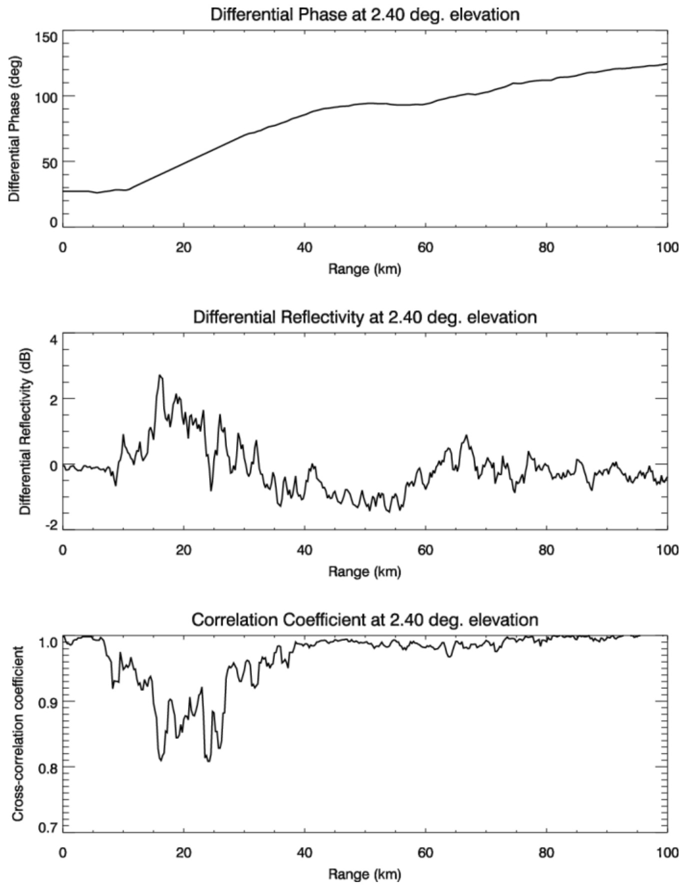

Fig.10: Line plot of Φ_{DP}, Z_{DR}, and ρ_{hv} (top, middle, bottom, respectively) as functions of range from KOKX, at 2233 UTC 8 February, at the 2.4° elevation, along the 144° azimuth.

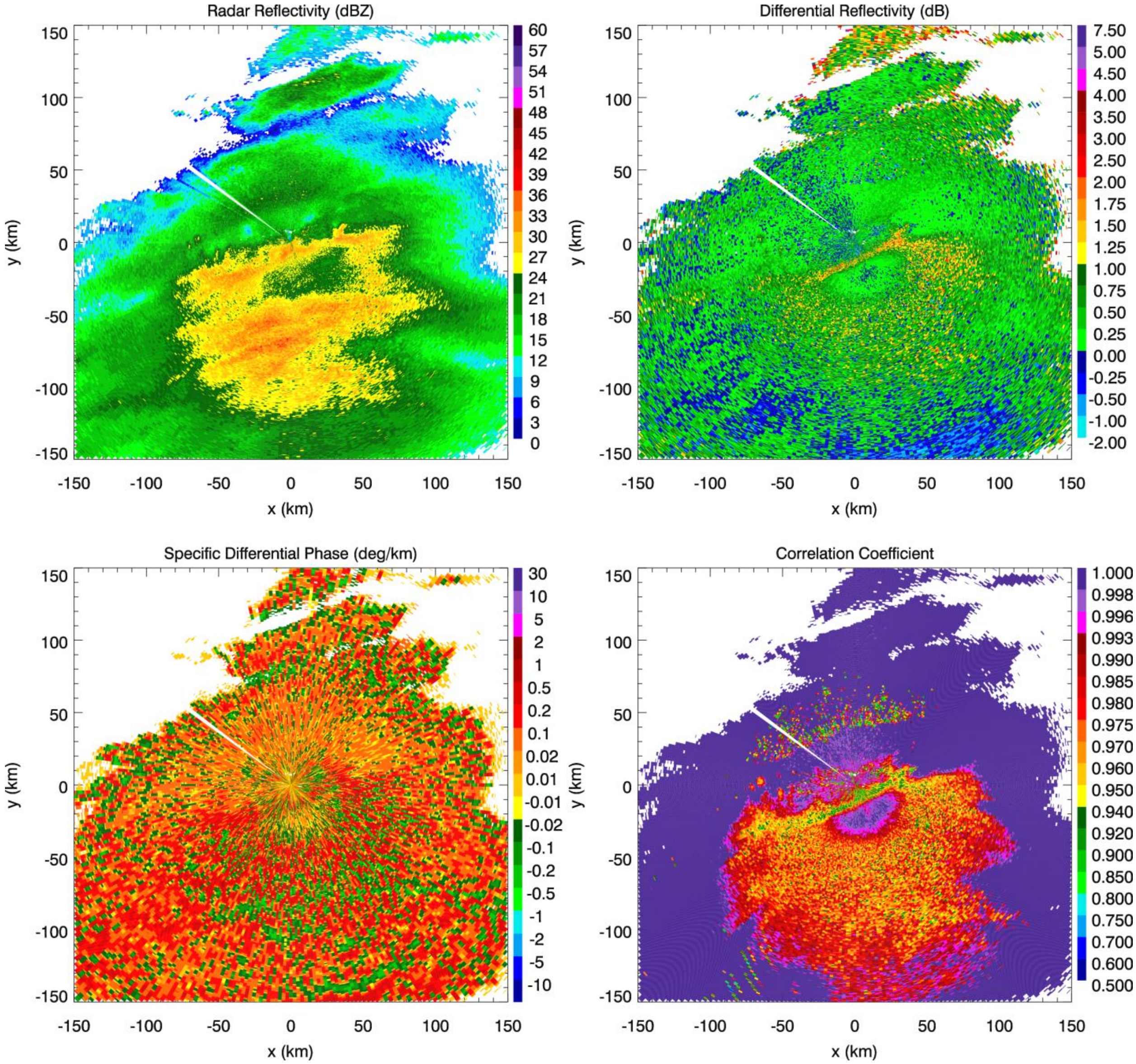

Fig.11: PPIs of Z_H, Z_{DR}, K_{DP}, and ρ_{hv} (top left/right, bottom left/right, respectively) at 1354 UTC 8 February 2013, at 0.5° elevation. The downward excursion of the MLBB to the surface (distinct in Z_{DR} and ρ_{hv}) was associated with a transition line of abrupt change in precipitation types at the surface.

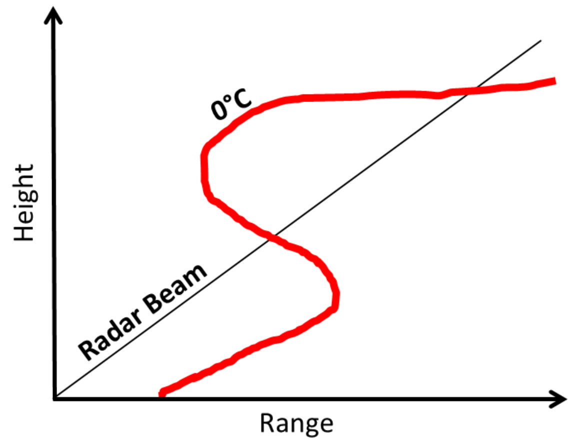

Fig.12: Range versus height illustration of the MLBB (0°C) sloping downward toward the surface. The radar beam increases in range and height from KOKX.

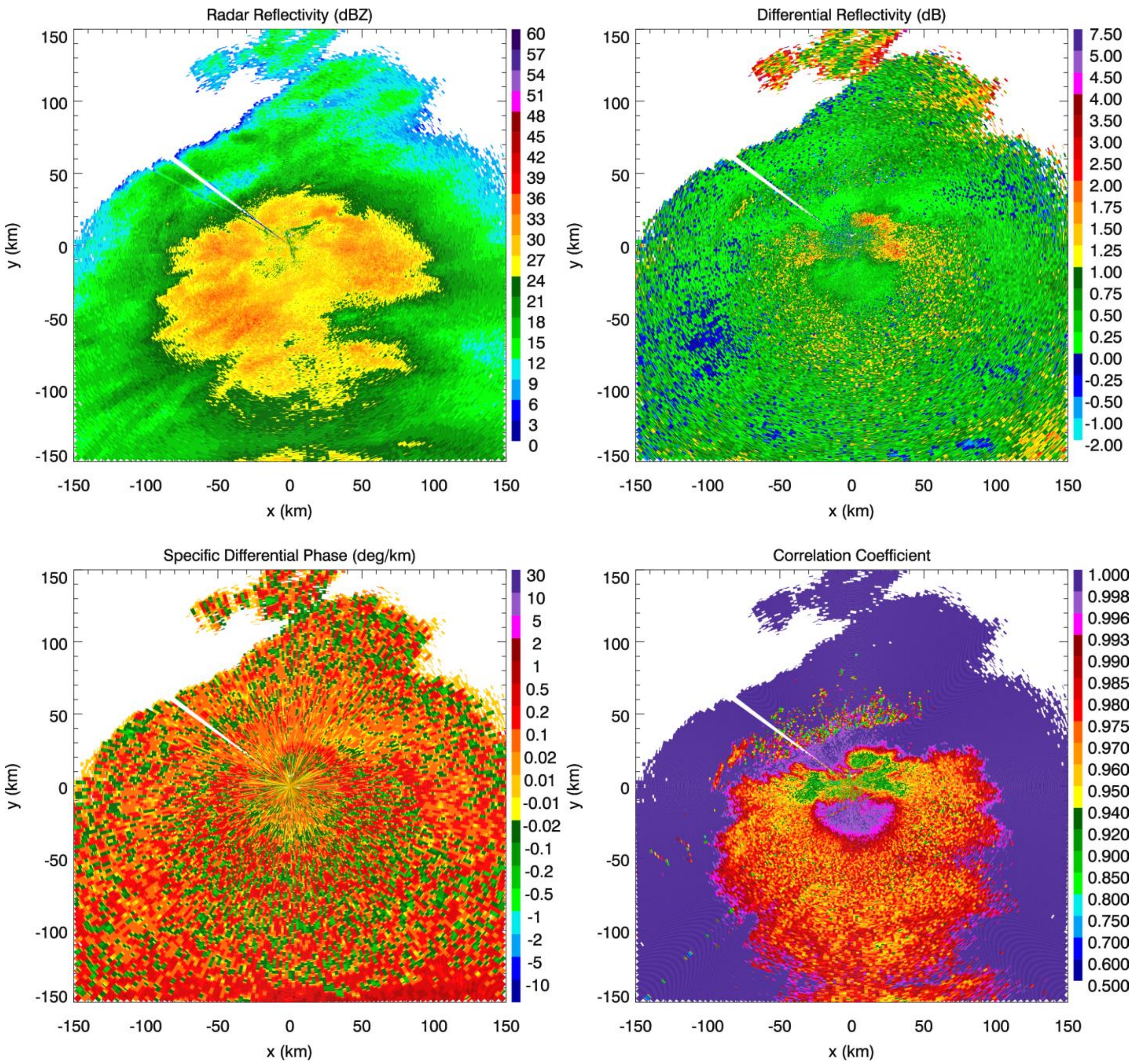

Fig.13: Same as Fig. 11, except at 1459 UTC 8 February.

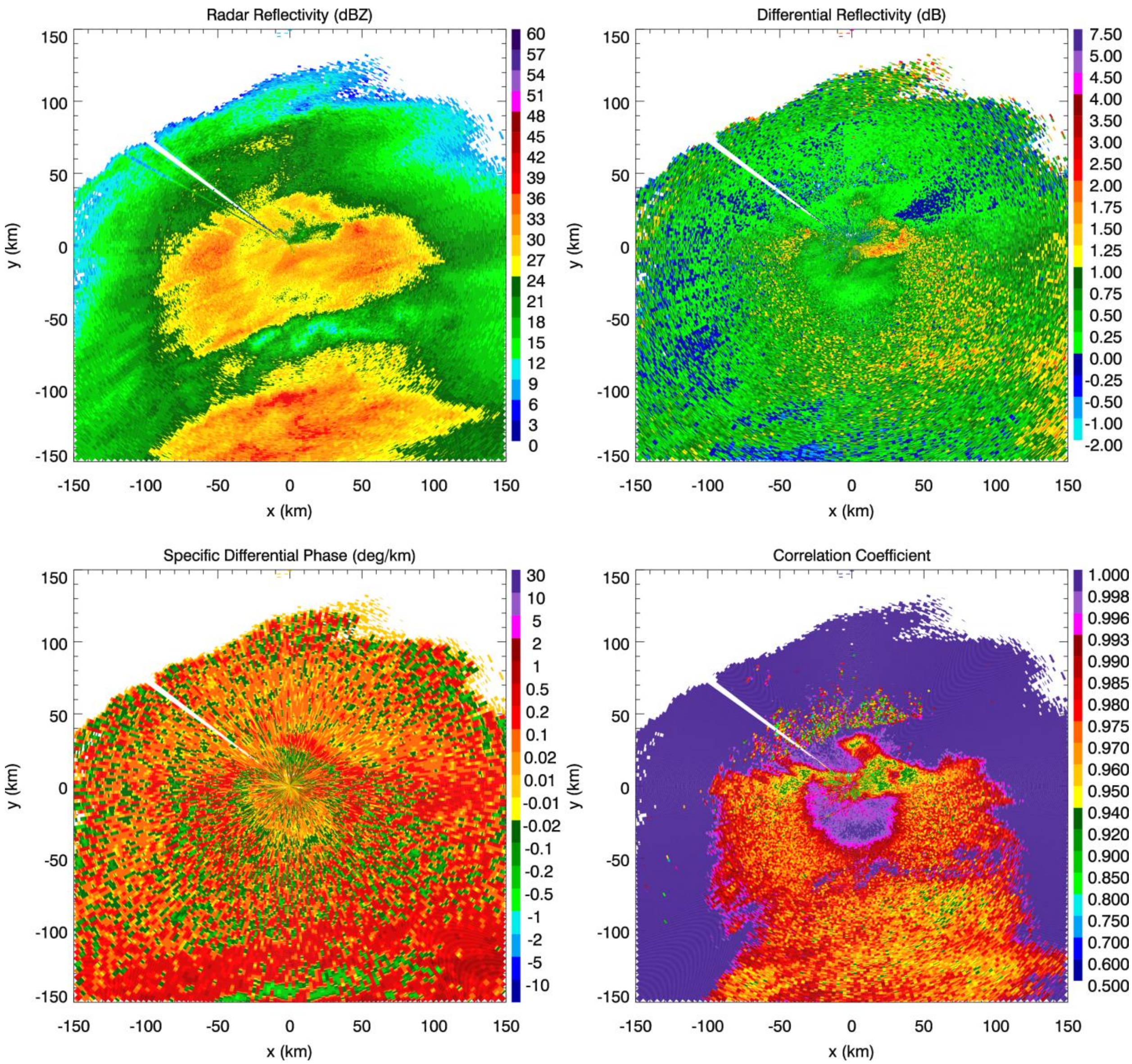

Fig.14: Same as Fig. 11, except at 1557 UTC 8 February.

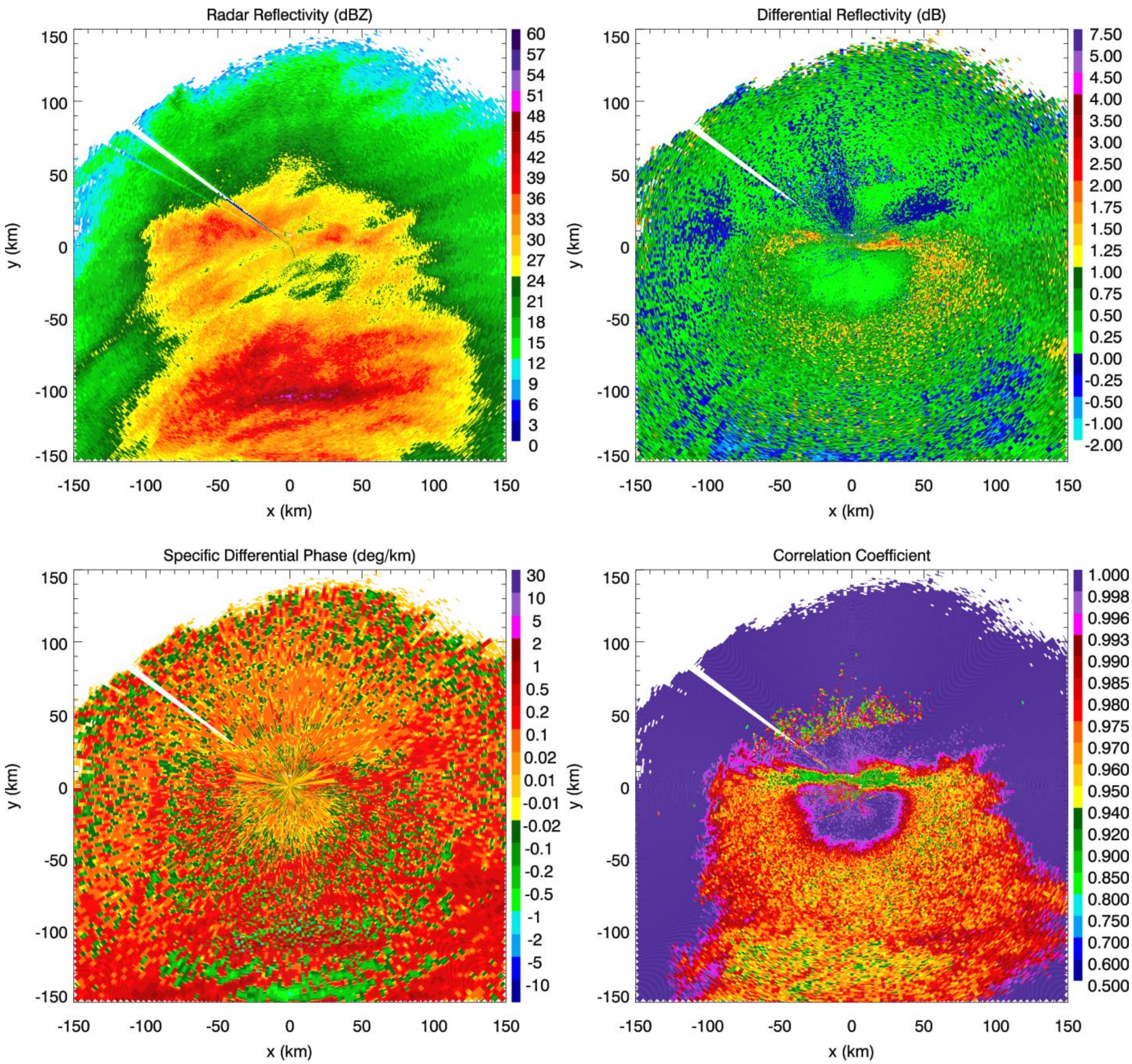

Fig.15: Same as Fig. 11, except at 1659 UTC 8 February.

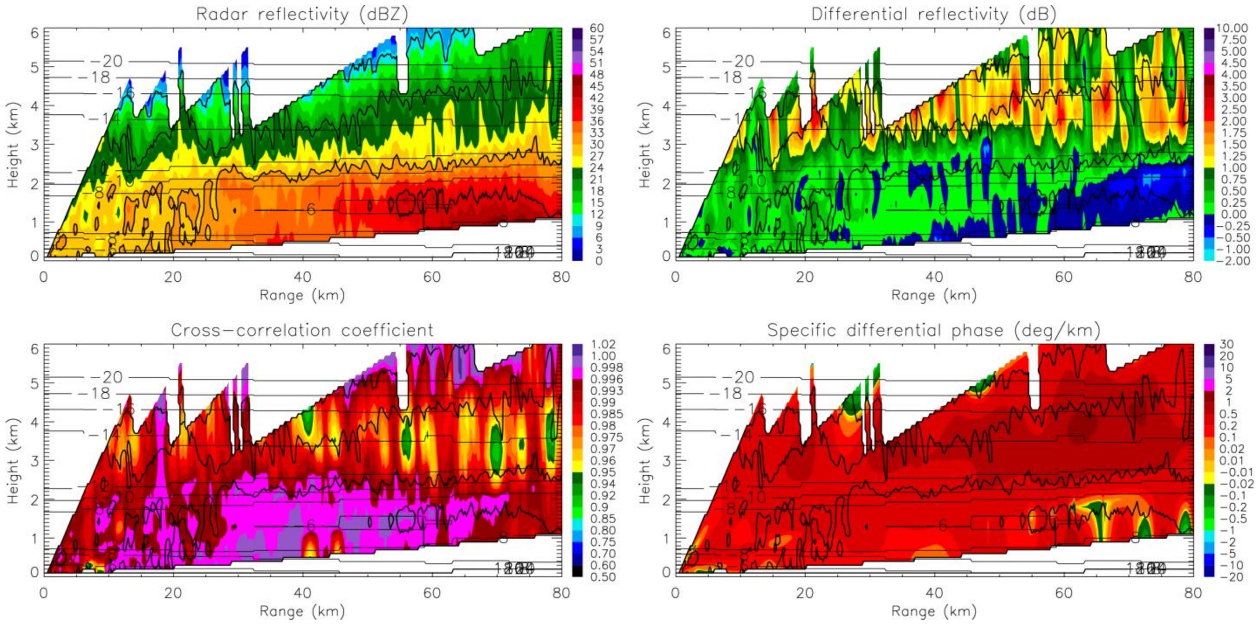

Fig.16: Same as Fig. 4, except at 0305 UTC 9 February, at 0° azimuth.

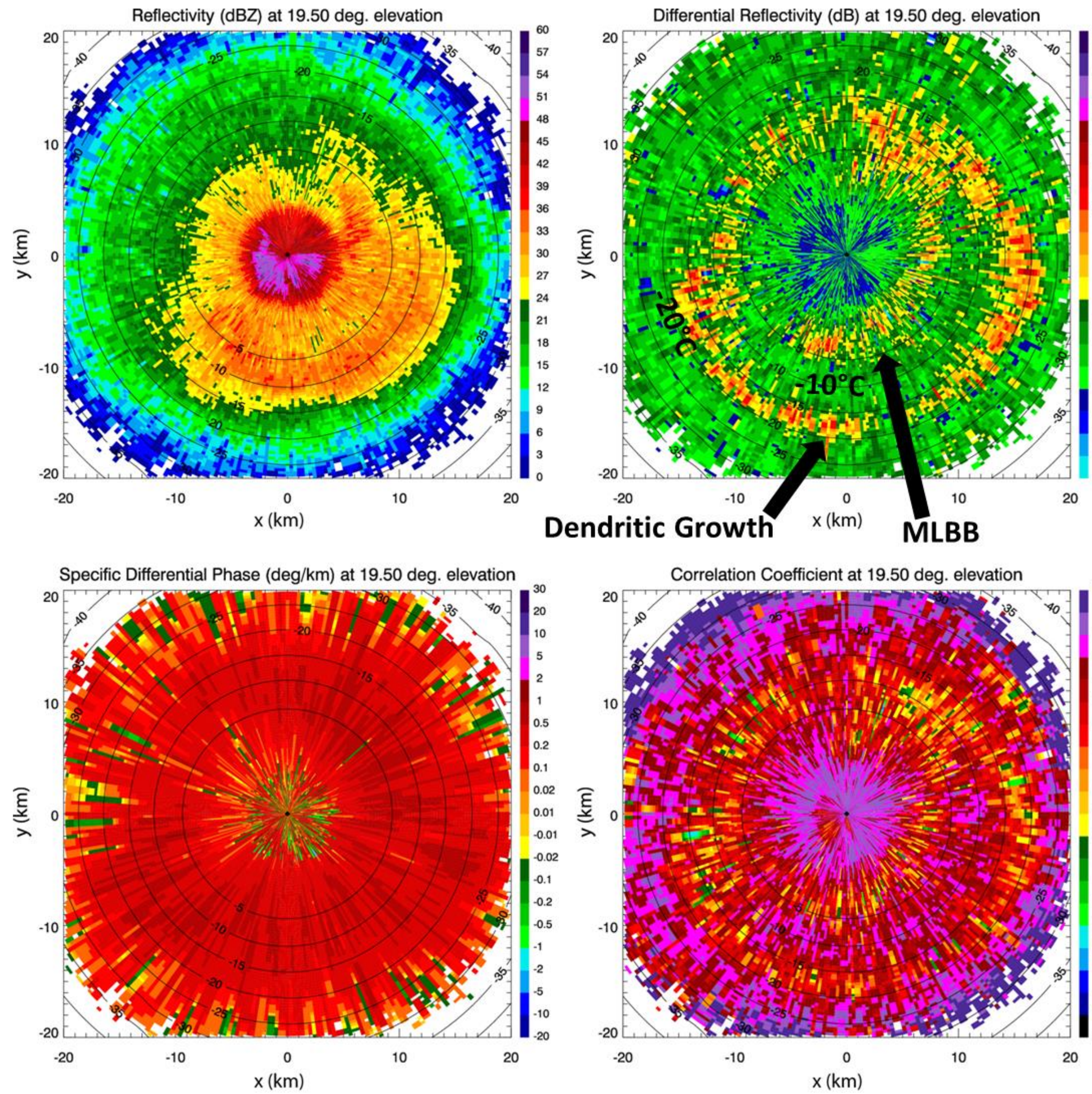

Fig.17: PPIs of Z_H, Z_{DR}, K_{DP}, and ρ_{hv} (top left/right, bottom left/right, respectively) at 2106 UTC 8 February 2013, at 19.5° elevation. Contours of RAP model wet-bulb temperatures on the conical surface are overlaid. Double rings of enhanced Z_{DR}, reduced ρ_{hv}, and slightly enhanced K_{DP} encircled KOKX; the outer ring indicates the dendritic growth layer, while the inner ring indicates the MLBB. This signature preceded the rapid increase in Z_H near the surface by less than one hour.

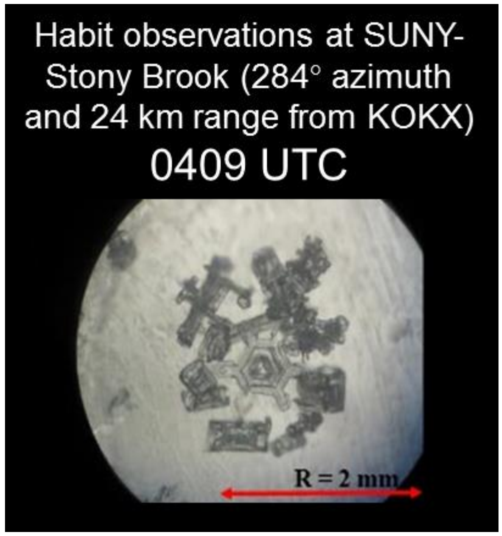

Fig.18: Image of a lightly-rimed dendritic ice crystal, observed at the surface at 0049 UTC 9 February at SBNY (Ganetis et al. 2013).

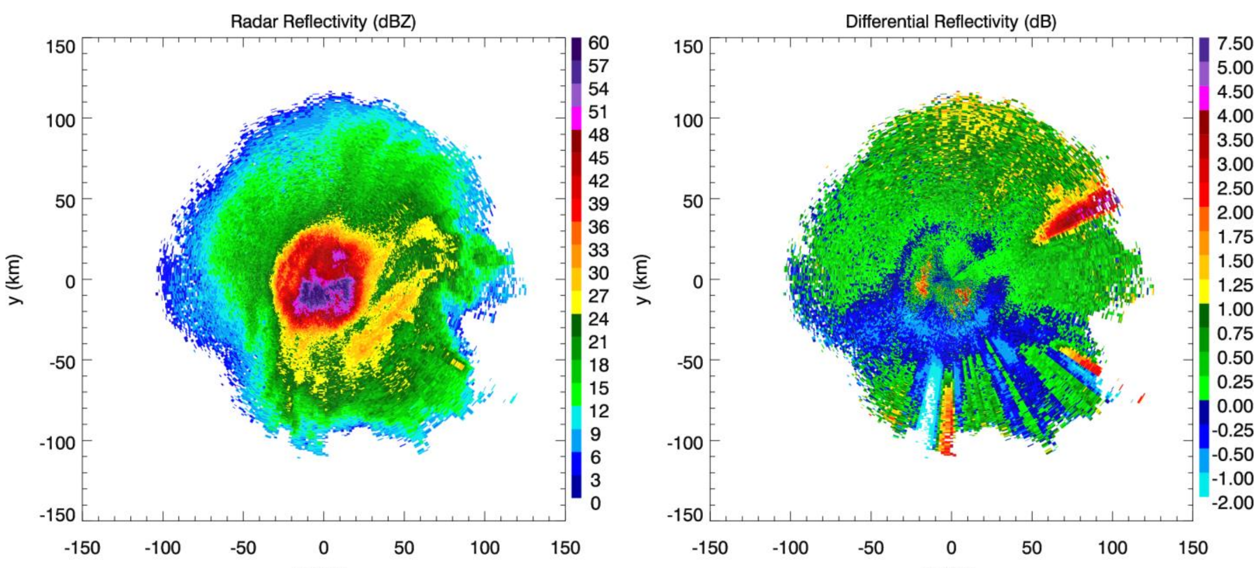

Fig.19: PPIs of Z_H (left) and Z_{DR} (right) at 2314 UTC 8 February, at 3.34° elevation. Depolarization streaks are indicated by the radial streaks of positive and negative Z_{DR}.

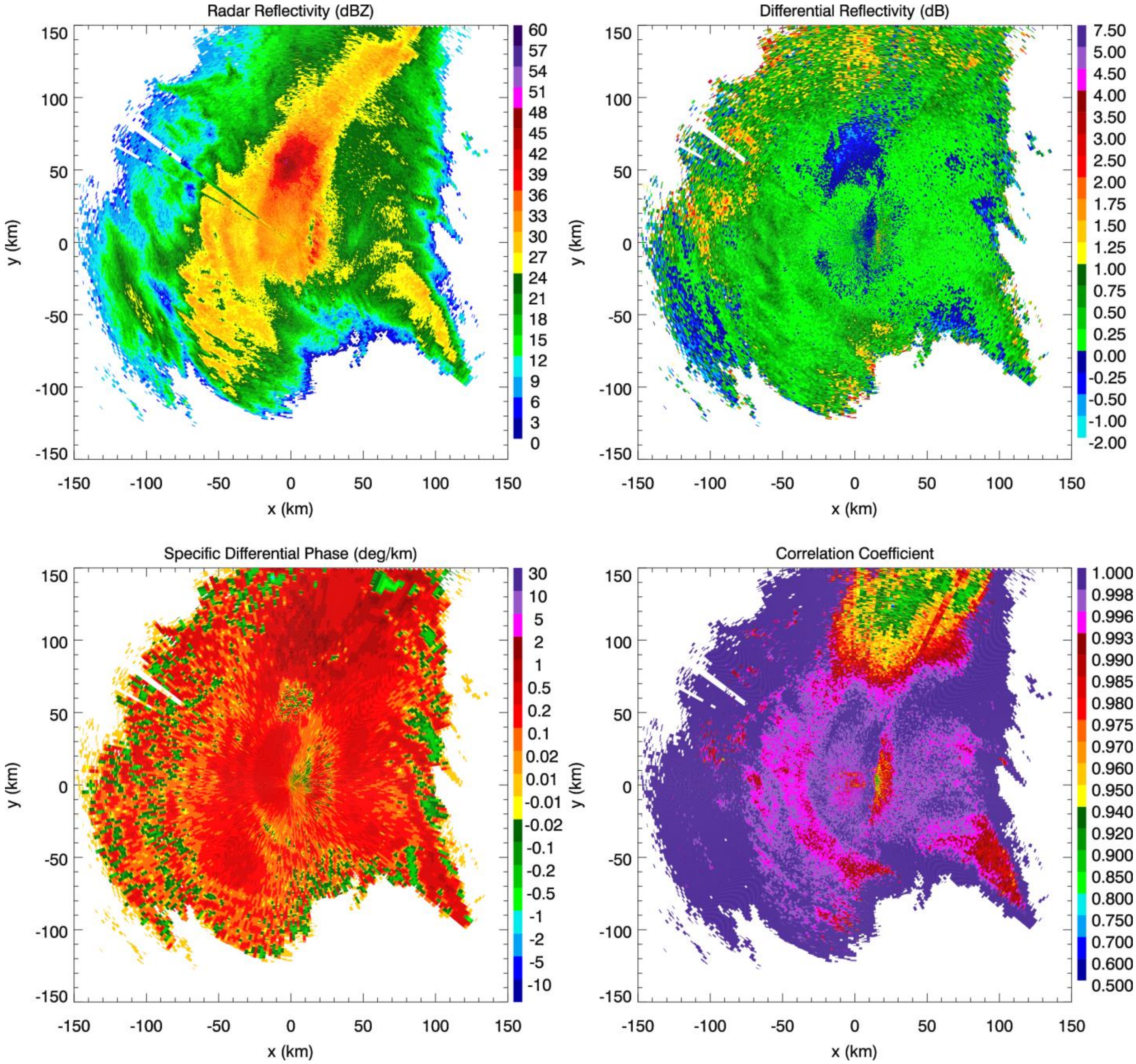

Fig.20: Same as Fig. 6, except at 0259 UTC 9 February. Non-uniform beam filling was indicated by the wedge of radial streaks of reduced ρ_{hv}.

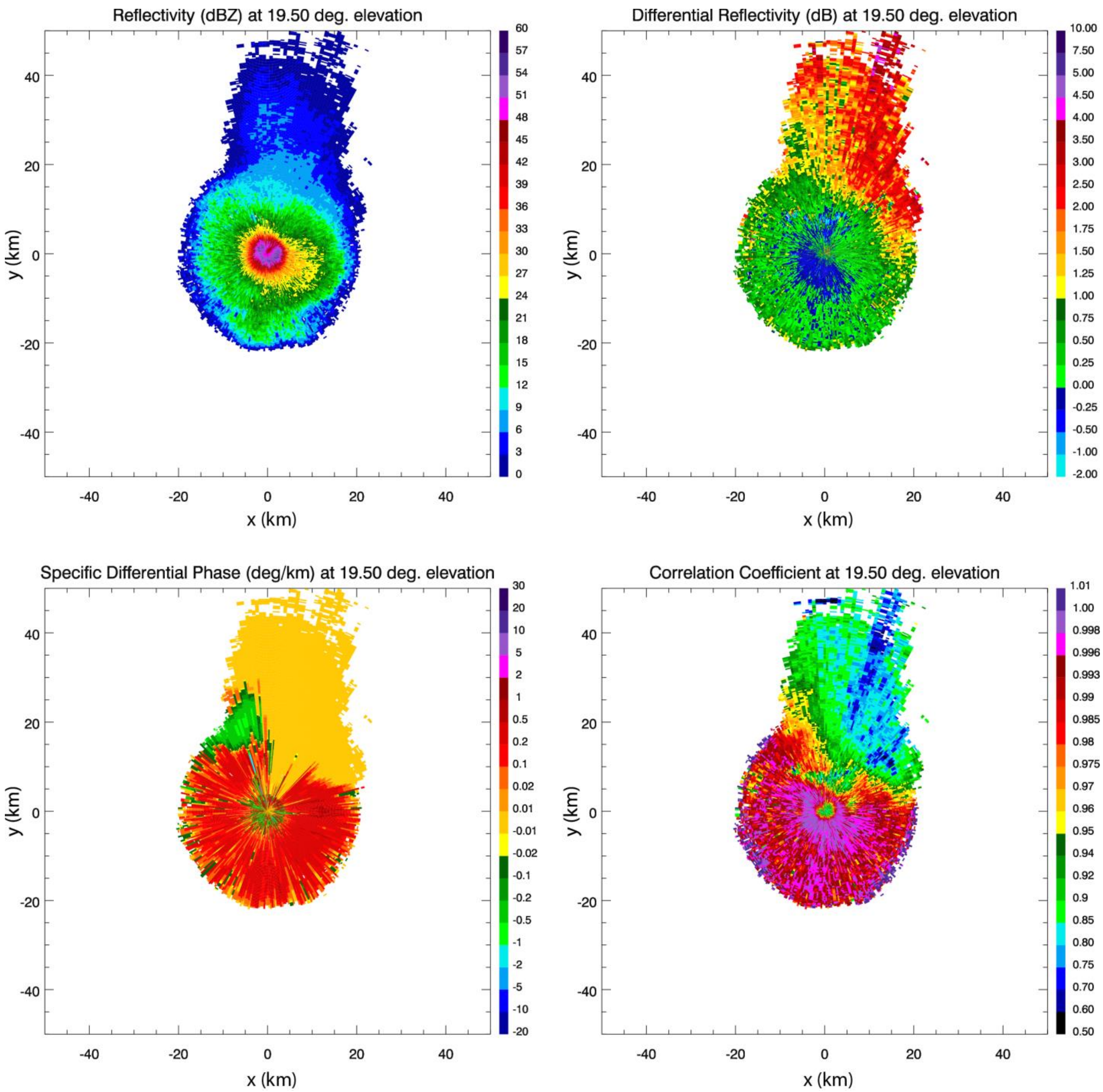

Fig.21: PPIs of Z_H, Z_{DR}, K_{DP}, and ρ_{hv} (top left/right, bottom left/right, respectively) at 0108 UTC 9 February, at 19.5° elevation. The "snow flare" was revealed by enhanced values of ρ_{hv} and Z_{DR}, collocated with low Z_H and moderate K_{DP}, flaring outward from KOKX. This artificial signature was associated with very large snowflakes, ice pellets, and "anonymous" ice hydrometeors at the surface.